Springer

KSME

Journal of Mechanical Science and Technology 33 (8) (2019) 3795~3802
www.springerlink.com/content/1738-494x(Print)/1976-3824(Online)
DOI 10.1007/s12206-019-0722-2

Formability and forming force in incremental sheet forming of AA7075-T6 at different temperatures †

Xiao Xiao[1], Chan-Il Kim[2], Xiao-Dong Lv[3], Tae-Seog Hwang [4] and Young-Suk Kim[1,*]

[1]*School of Mechanical Engineering, Kyungpook National University, Daegu, Korea*
[2]*Institute of Mechanical Engineering Technology, Kyungpook National University, Daegu, Korea*
[3]*School of Mechanical Engineering and Automation, Beihang University, Beijing, China*
[4]*Research Center, Hyoseng Electric Co., Ltd, Busan, Korea*

(Manuscript Received August 22, 2018; Revised January 16, 2019; Accepted January 17, 2019)

Abstract

The AA7075-T6 sheet recently received attention, owing to its low weight and strength for use fabricating automotive parts (e.g., body, motor case). Owing to its low ductility and high strength at room temperature, it is difficult to form; a heating process is required. In this paper we investigate the mechanical properties of a 1.0-mm-thick AA7075-T6 sheet at different temperatures via an uniaxial tensile test, examining the forming characteristics of incremental sheet forming (ISF) at different temperatures. In the ISF experiment, a sheet clamped on a fixed die was heated and maintained at the designed temperature. The forming force was measured by an in situ force monitoring system. The forming parameters included tool diameter, vertical step, temperature, and feed speed. Vertical step and temperature were selected at three levels for experimental design. The formability was evaluated by varying the shapes of wall-angle conical frustums. When the temperature increased to 200 °C, the formability increased dramatically. The fracture-forming limit curve in ISF was defined for this material at different temperatures. This fracture criterion was loaded into ABAQUS software to predict fracture. The comparison between experimental and finite-element method simulation shows good agreement.

Keywords: AA7075-T6; Incremental sheet forming; Forming force; Formability; Finite element method; High temperature

1. Introduction

Incremental sheet forming (ISF) is a flexible sheet-forming process that has gained significant interest since the pioneering work of Iseki et al. [1]. ISF is a highly localized deformation process in which a tool is programmed to move along to a certain path to create the desired part geometry. A simple incremental sheet-forming process to manufacture a truncated cone is depicted in Fig. 1 [2]. The workpiece/blank is clamped with a fixture. A pin-like tool is programmed to follow the circumference of a circle. After completing the circle, the tool steps down and towards the center to start a new circular pass. After a number of passes, a truncated cone can be generated. Without complex tools and dies, the process can form various part geometries directly from computer-aided design models and computer numerical control codes. The process has great potential for rapid parts prototyping requiring small quantities. Additionally, it is known that ISF can significantly increase the formability of the sheet metal work-piece [3]. Furthermore,

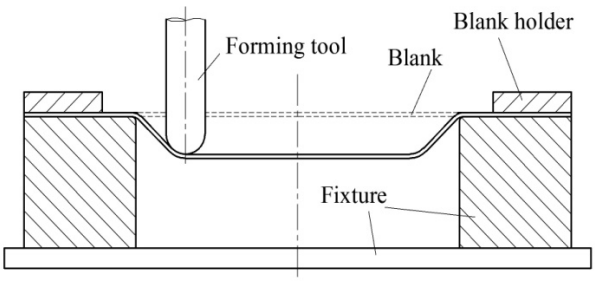

Fig. 1. Single point incremental forming for truncated cone.

to enhance formability, several ISF schemes (e.g., water-jet ISF [4], micro ISF [5], robot-assisted ISF [6] and heat-assisted ISF [7]) have been proposed.

The forming parameters of ISF include the forming angle, θ, tool diameter, vertical-step depth, horizontal-step depth, tool rotation speed (spin speed), ω, feed speed, s, sheet thickness, t, and temperature. Selection of the forming parameters results in the final part appearance. The forming angle strongly affects part accuracy. Forming step size decides the part-surface quality. Tool speed is related to heat generation. Contact between the tool and the sheet should be lubricated to reduce

*Corresponding author. Tel.: +82 539505580, Fax.: +82 539506550
E-mail address: caekim@knu.ac.kr
† This paper was presented at ETME 2018, Ramada Plaza Jeju Hotel, Jeju, Korea, August 19-22, 2018. Recommended by Guest Editor Maenghyo Cho.

frictional heat.

Prediction of ISF forming forces is especially important when using adapted machinery not designed for the forming process, such as milling centers and robots. It was demonstrated by Durante et al. [6] that the predominant force in ISF was developed in the axial direction of the. This generally is not the case in milling. Consequently, an accurate estimation of the maximum axial force developed during the forming process was required to ensure the safe utilization of the hardware.

In recent years, with energy and environmental issues becoming more critical, reducing emissions has become a common goal of the automotive industry. Automotive lightweight technology is an important way to solve the problems of saving resources and reducing pollution. Lightweight materials are not only needed for large parts (e.g., car body), it is suitable for small parts (e.g., motor case). Compared with the steel plates, aluminum plates with low density, high strength, corrosion resistance, etc., have become an important lightweight vehicle technology material. Because of fuel economy requirements, automobile manufacturers use high-strength aluminum alloy material. Unlike steel, aluminum alloy sheets at room temperature show poor formability, it is difficult to use the traditional cold-forming process. However, with an increase of temperature, formability can be significantly improved [8]. This study shows that the elongation of aluminum sheets increases while the tensile strength and yield point decrease with temperature increments. Thus, at high temperatures, not only the forming force can be reduced, but the formability can also be improved.

As mentioned, many researches used deep-drawing, hot-stamping technology for AA7075 aluminum [9-11], and the formability of AA7075 aluminum alloy sheet did not improve when the temperature was lower than a certain critical point. However, the formability of AA7075 aluminum alloy sheet obviously improved when the temperature was higher than this critical temperature. This shows that the AA7075 sheet has a strong sensitivity to temperature change within a certain range. However, the experimental research on the thermo-forming of AA7075 aluminum via the incremental sheet-forming process is still relatively small. Thus, it is necessary to confirm the influence of temperature on incremental sheet forming.

This study adopts AA7075 aluminum alloy sheets, provided in T6 temper conditions, having practical and wide industrial application because of their higher formability compared with the other temper conditions. The mechanical properties of 1.0-mm-thick AA7075-T6 sheet was clarified at different temperature by first using a uniaxial tensile test. Then, the maximum forming force and formability of this material in ISF process at different temperatures were defined experimentally. The forming limit curves at fracture for ISF were also defined at different temperatures. Finally, the finite-element method (FEM) model, provided by ABAQUS/Explicit software for the ISF process, was built to successfully predict the performance of the ISF process, compared to experiment results.

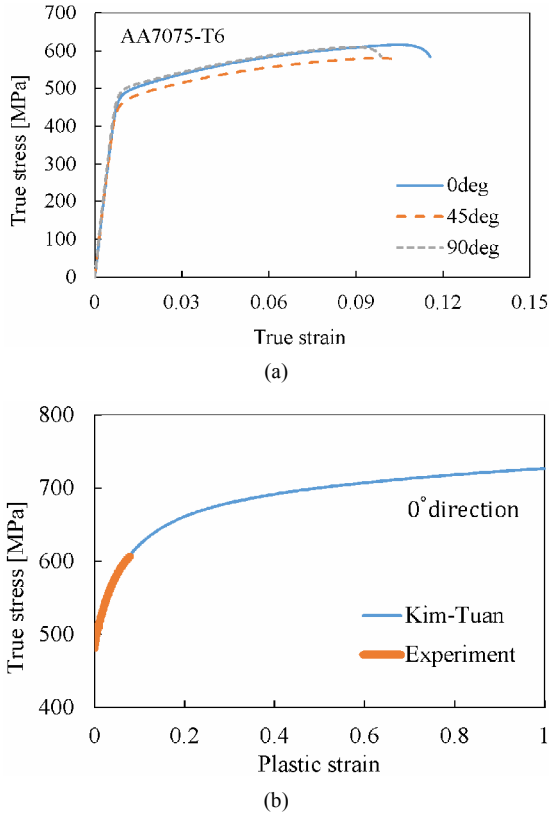

Fig. 2. (a) Stress-strain curve of AA7075-T6 sheet; (b) curve-fitting, using the Kim-Tuan equation at room temperature.

2. Materials and experiment methods

2.1 Material properties by uniaxial tensile tests

For a 1.0-mm-thick AA7075-T6 sheet, a series of uniaxial tensile specimens in three directions of 0°, 45° and 90°, with respect to the rolling direction, were performed following the ASTM-8 standard at a constant tensile speed of 10 mm/min with a gauge length of 50 mm. The laser-cutting method was applied to prepare the specimens to increase the accuracy and reduce the effect of the cutting process on the specimen surfaces.

Via tensile tests, the mechanical properties (e.g., Young modulus, yield stress, elongation and anisotropic parameters) were obtained, as presented in Table 1. Fig. 2(a) shows the true-stress-true-strain curve of the AA7075-T6. The maximum strain observed from the uniaxial tensile test was about 0.12. It is well established that the tested material, however, undergoes a large deformation during incremental forming. This may generate a high level of strain (e.g., $\varepsilon = 1.0$). Therefore, the hardening function should provide an acceptable estimation for stress-strain relation beyond the maximum observed strain or post-necking prediction. The Kim-Tuan hardening model has been proven a good choice for this purpose, because it provides better prediction for post-necking behaviors

Table 1. Mechanical properties of material AA7075-T6 with three directions.

Direction	0°	45°	90°
Young modulus [GPa]	67	69	75
Yield stress [MPa]	477.35	453.99	485.14
Elongation [%]	13.47	11.01	10.84
R-value	0.79	1.12	0.81
K_T [MPa]	341.2	366.72	364.62
m	0.51	0.49	0.45
c	85.42	83.56	82.68

of various sheet metals [12]. Therefore, this study adopts the Kim-Tuan hardening model (see Eq. (1)) to describe the stress-strain relation for the tested material. Also, see Fig. 2(b).

$$\sigma = \sigma_Y + K_T\left(\varepsilon + \varepsilon_0\right)^m \left(1 - \exp\left(-c\varepsilon\right)\right). \quad (1)$$

where K_T, m and c are the parameters of the proposed equation, and m is the dependent parameter calculated by

$$m = \frac{\sigma^*}{\sigma^* - \sigma_0}\left(\varepsilon^* + \varepsilon_0\right) \quad (2)$$

where (ε^*, σ^*) is the maximum tensile force point, and (ε_0, σ_0) is the initial yield point in the true-stress-true-strain curve. The parameter, m, is a dependent parameter whose value does not depend on the other parameters. Therefore, the value of parameters K_T and c in the Kim-Tuan model can be found using the curve-fitting tool available on some optimization packages, such as Excel or Matlab.

2.2 Effect of temperature on mechanical properties

High-temperature tensile tests were performed in a universal testing machine. A three-dimensional (3D) digital image correlation (DIC) system was used to measure the strain during the process. The testing environment was enclosed in a designed heating system, which can heat the specimens to 500 °C (Fig. 3).

The true-stress-true-strain relationships for different temperatures (Fig. 4) show that AA7075-T6 has a noticeably higher ultimate strength and lower total elongation at room temperature.

Table 2 shows the mechanical properties of material AA7075-T6 at different temperatures. There is no significant change when the temperature is between 20 °C and 80 °C. However, there is a clear decrease in stress and an increase in elongation at temperatures ranging from 80 °C to 200 °C.

2.3 Formability and forming force measurement by ISF

In the experiments, AA7075-T6 specimen with a size of 130 mm × 130 mm was cut to be formed using varying wall-angle conical frustums (VWACF) to check the formability

Table 2. Mechanical properties of material AA7075-T6 at different temperature.

Temperature	20 °C	80 °C	140 °C	200 °C
Young modulus [GPa]	67	71	62	58
Yield stress [MPa]	477.35	417.1	366.26	281.93
Elongation [%]	13.47	14.41	17.93	20.94
K_T [MPa]	341.2	358.43	169.46	163.32
m	0.51	0.35	0.21	0.27
c	85.42	569.98	507.88	427.26

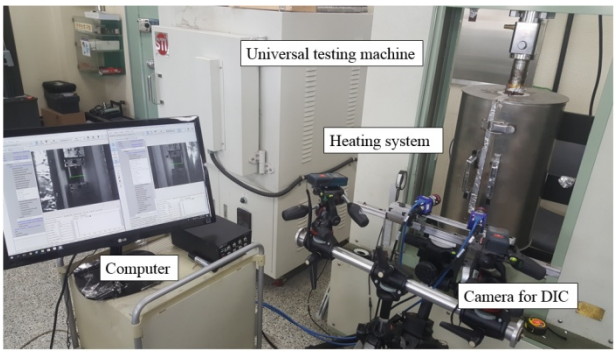

Fig. 3. Uniaxial tensile test with heating system and 3D-DIC system.

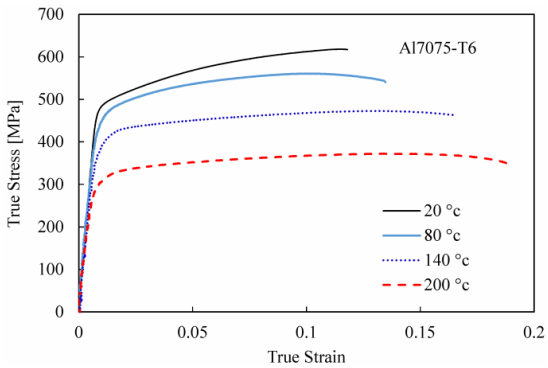

Fig. 4. True stress-true strain curves of AA7075-T6 at several elevated temperatures.

[13-16] (see Fig. 5). The VWACF for experiments used the opening diameter of 80 mm, a depth of 70 mm, a generatrix radius of 80 mm, an initial wall angle of 40°, and an end wall angle of 90°. The arbitrary wall angle (θ) continuously increases along the forming depth, thus inducing a proportional amount of wall thinning, leading to sheet fracture after many passes. The wall angle corresponding to the fracture point is regarded as θ and is calculated using Eqs. (3) and (4). r is the tool radius, d is the forming depth at fracture, L is the overall depth of the part, and R is the test-shape radius.

$$H = L - d + r. \quad (3)$$

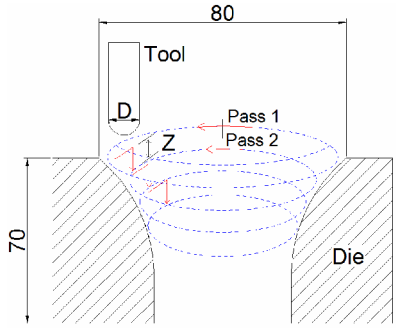

Fig. 5. Varying wall angle conical frustum for experiments (D: Tool diameter; Z: Vertical step depth).

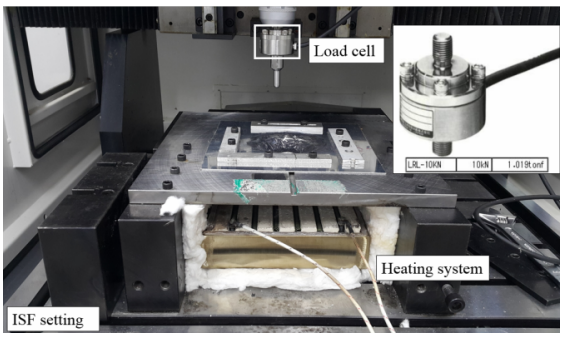

Fig. 6. Process setting of study and load cell.

$$\theta = \frac{\pi}{2} - \arcsin\left(\frac{H}{r+R}\right). \quad (4)$$

In all experiments, a hemispherical end tool with a 10-mm diameter, made from high-speed steel (HSS4341), was employed. The feed rate of the tool was fixed at 200 mm/min. mechanical grease was used to eliminate friction between the tool and the sheet. A compact tensile compression load cell was mounted in the tool holder to measure the forming forces occurring during the ISF process. The forces were acquired using a DaqBoard 505 data acquisition card and DaqView 9.0.0 software. A real-time monitoring heating system was used (see Fig. 6).

To determine the effect of temperature in the ISF process, four elevated levels of differing temperatures were set for ISF experimental tensile tests, along with other process parameters. The selected levels are shown in Table 3. Table 4 shows the experimental conditions for 12 experiments.

3. Results and discussion

3.1 Formability

Fig. 7 shows some of the experimental results. It can be seen that, in the experimental range, specimens can be formed to a certain depth before fracture. The fracture depth is measured to calculate the maximum forming angle via Eqs. (3) and (4).

The maximum forming angle for each experiment is shown in Table 5.

Table 3. Process parameters and their levers in ISF experiments.

Parameter	Description	Level 1	Level 2	Level 3	Level 4
T	Temperature (°C)	20	80	140	200
Z	Vertical step depth (mm)	0.3	0.5	0.7	-
D	Tool diameter (mm)	10	-	-	-
S	Feed speed (mm/min)	200	-	-	-

Table 4. Experimental conditions for ISF processes.

Experiment	T (°C)	Z (mm)	D (mm)	S (mm/min)
1	20	0.3	10	200
2	20	0.5	10	200
3	20	0.7	10	200
4	80	0.3	10	200
5	80	0.5	10	200
6	80	0.7	10	200
7	140	0.3	10	200
8	140	0.5	10	200
9	140	0.7	10	200
10	200	0.3	10	200
11	200	0.5	10	200
12	200	0.7	10	200

The effect of the temperature on formability is shown in Fig. 8. At room temperature, the maximum forming angle of the AA7075-T6 sheet in ISF was around 50°. As temperature increased, the maximum forming angle became higher. From 20 °C to 80 °C, there was no significant change in maximum forming angle. At 200 °C, the maximum forming angle increased significantly until it was greater than 80°. Thus, the formability increase is remarkable with the temperature increase. However, vertical step depth also has this effect on formability. In all temperature levels, the vertical step depth is bigger, and the maximum forming angle is lower. Thus, the vertical step depth increase leads to the decrease of formability.

3.2 Forming force

The influence of temperature on resultant forming forces was then compared. Figs. 9-11 show the results of the forming forces in Z-directions (Fz), measured by the load cell. It can be observed that the forming force gradually increased as the number of passes increased. After about 10 passes, at the depth of 5-7 mm, “steady-state” forces were reached. It was also observed that the time required to complete a pass gradually shortened, because the perimeter of the VWACF decreased as the depth increased. Nevertheless, the force pattern and the peak forces repeated until the full depth was reached.

Table 6 shows the max-forming forces in the Z-directions

(a) D = 10 mm, S = 200 mm/min, Z = 0.5 mm, T = 20 °C

(b) D = 10 mm, S = 200 mm/min, Z = 0.5 mm, T = 80 °C

(c) D = 10 mm, S = 200 mm/min, Z = 0.5 mm, T = 140 °C

(d) D = 10 mm, S = 200 mm/min, Z = 0.5 mm, T = 200 °C

Fig. 7. Some formed varying wall angle conical frustums at different forming conditions.

during the forming process.

The effect of temperature on the maximum forming force is shown in Fig. 12. At room temperature, the maximum forming force in the Z-direction of the AA7075-T6 sheet during ISF was about 1900 N. Until 140 °C, the forming forces reduced slightly as the temperature increase. However when temperature reached 200 °C, the forming force decreased significantly, until it reached 1300 N. Thus, temperature had a large effect on the max forming force of AA7075-T6 in the ISF process.

For the vertical step depth, as the temperature increased, the vertical step depth increased, whereas the maximum forming force increased.

Table 5. Maximum forming angle in each experiment.

Temperature (°C)	Maximum forming angle (°)		
	Z = 0.3 mm	Z = 0.5 mm	Z = 0.7 mm
20	51.97	50.50	49.15
80	58.67	56.90	54.26
140	74.09	70.97	67.16
200	84.26	82.75	81.37

Table 6. Maximum forming forces in each experiment.

Temperature (°C)	Max forming force (N)		
	Z = 0.3 mm	Z = 0.5 mm	Z = 0.7 mm
20	1900	1930	1970
80	1700	1800	1700
140	1610	1660	1700
200	1300	1350	1400

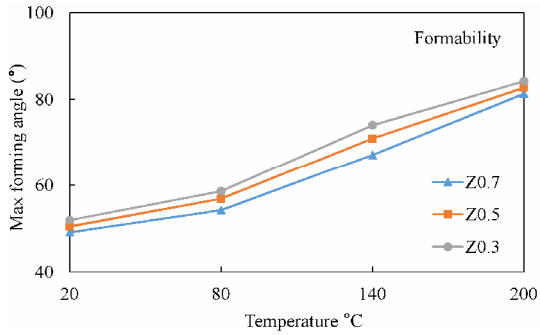

Fig. 8. Effect of the input parameter to the formability.

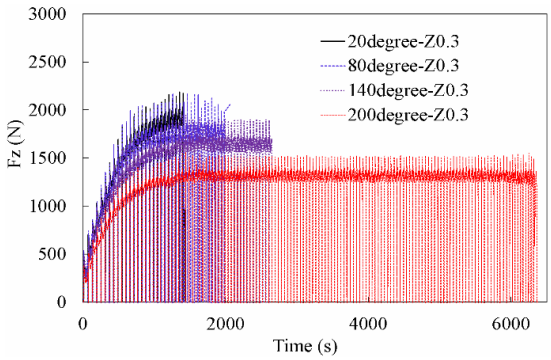

Fig. 9. Forming force in the Z-directions for the VWACF with vertical step depth of 0.3 mm at different temperatures.

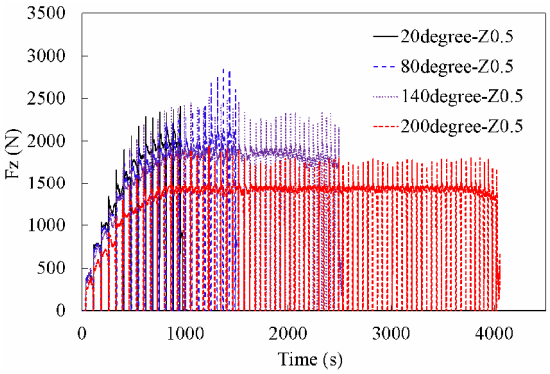

Fig. 10. Forming force in the Z-directions for the VWACF with vertical step depth of 0.5 mm at different temperatures.

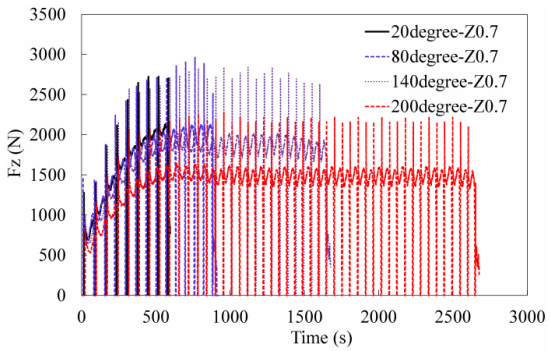

Fig. 11. Forming force in the Z-directions for the VWACF with vertical step depth of 0.7 mm at different temperatures.

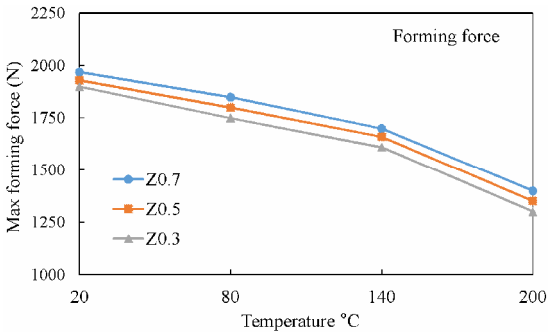

Fig. 12. Effect of the input parameter to the forming force.

4. Finite element simulation

4.1 FEM model

The FEM of ABAQUS/Explicit v. 6.14 is shown in Fig. 13. The full model was used to ensure the correct results, because the symmetry condition does not correctly describe the mechanical deformation of the sheet during the forming process. The AA7075-T6 sheet was meshed using a square shape, S4R type with a size of 1 mm. It was integrated via Gauss integration with five points in the through-thickness direction. The fixed die was modeled as a discrete rigid body and meshed with the R3D4 element. The tool with a diameter of 10 mm

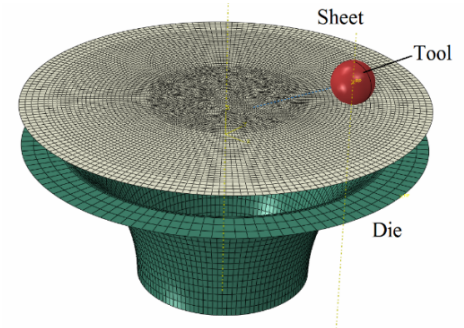

Fig. 13. FEM model by ABAQUS/Explicit version 6.14.

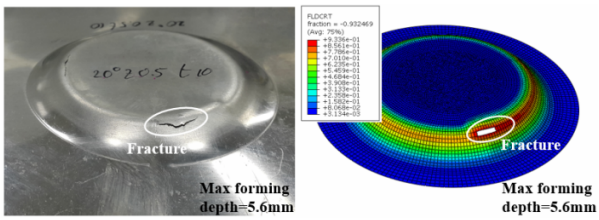

(a)

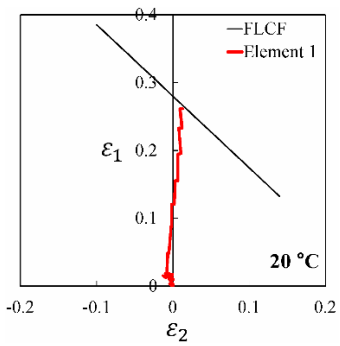

(b)

Fig. 14. (a) Fracture prediction by ABAQUS/Explicit for the case of room temperature; (b) strain evolution for the element next to the deleted element in the simulation for the case of 20 °C.

was modeled as analytically rigid. An elastic-plastic model was selected, and the material properties, such as Young's modulus, Poisson's ratio, and the density, were inputted. The flow curve of the Kim-Tuan equation and the Hill48 yield function were used in the simulation of the AA7075-T6 sheet.

Additionally, the forming limit diagram criterion (FLDCRT) was applied to predict the fracture phenomena during the forming process [17, 18]. The forming limit curve at fracture (FLCF) for material AA7075-T6 at room temperature is described as $\varepsilon_1 = -1.055\,\varepsilon_2 + 0.28$. At 200 °C, it is described as $\varepsilon_1 = -1.056\,\varepsilon_2 + 1.204$. In simulation, the fracture is considered to occur at one element when its FLDCRT value, defined by the ratio of the major strains (ε_1) and the FLC values (ε_1 FLCF) at the same point for the minor strains (ε_2), reaches to the unit value. In this simulation, the FLDCRT value at elements was over the unit, and the elements were deleted (see Figs. 14(a)-15(a)).

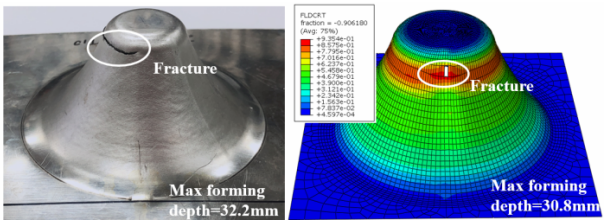

(a)

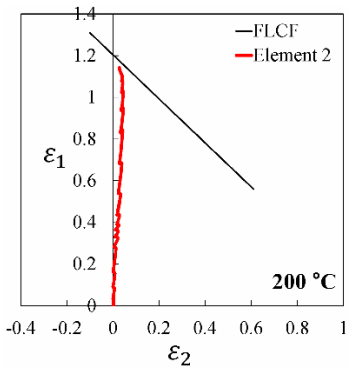

(b)

Fig. 15. (a) Fracture prediction by ABAQUS/Explicit for the case of 200 °C; (b) strain evolution for the element next to the deleted element in the simulation for the case of 200 °C.

4.2 Comparison between FEM and experiment

Figs. 14(a) and 15(a) show the fracture prediction from FEA for two cases (i.e., room temperature and 200 ºC) compared to the experimental observations. The estimated forming depths at fracture were 5.6 mm and 30.8 mm for room temperature and 200 °C models, respectively. However, the experimentally measured forming depths were 5.6 mm and 32.2 mm respectively. Strain evolution for elements 1 and 2, next to the deleted element in the simulation for the case of 20 °C and 200 °C, are shown in Figs. 14(b) and 15(b), respectively. This shows that the element in the VWACF shape can be considered a plane-strain deformation. For both cases, the strain increased with the forming depth. When this value reaches FLCF value, the elements are deleted.

According to these figures, the FEA model provided well-matched results to the experimental one both by means of forming depth and failure position. In the case of room temperature, the FEM prediction gave the same result as the experiment. However, for the case of 200 °C, the FEM model gave a lower result with a 4.35 % error. This error may come from the changes to material properties caused by long-duration high temperature. Nevertheless, the prediction result is acceptable. It verifies the accuracy of the developed FEA model.

5. Conclusions

In this study, an experimental ISF was conducted to deform AA7075-T6 aluminum alloy sheets at different temperatures. Basic material properties were acquired to clarify the material behavior using tensile tests. Formability and forming forces were evaluated to understand the forming process mechanism at different temperatures. Some conclusions can be drawn, as follows:

(1) In the tensile test, as the temperature increased, the strength of the AA7075-T6 sheet continued to decrease, and the elongation increased. There was no significant change when temperature ranged from 20 °C to 80 °C. However, there was a clear decrease in stress and an increase in elongation at temperatures ranging from 80 °C to 200 °C.

(2) Formability in ISF increased remarkably with the temperature increase. At room temperature, the maximum forming angle of the AA7075-T6 sheet in ISF was around 50°. As temperature increased, the maximum forming angle became higher. From 20 °C to 100 °C, there was no significant change in maximum forming angle. At 200 °C, the maximum forming angle increased significantly until it was greater than 80°.

Vertical step depth also affected formability. A vertical step depth increase led to a decrease in formability.

(3) Temperature had strong effect to the maximum forming force of the AA7075-T6 during the ISF process. At room temperature, the maximum forming force in the Z-direction of the AA7075-T6 sheet during ISF was about 1900 N. Until 140 °C, the forming forces reduced slightly as the temperature increased. However, when temperature reached 200 °C, the forming force decreased significantly, until it reached 1300 N.

For the vertical step depth, at room temperature, as the temperature increased, the vertical step depth increased, and the max forming force increased.

(4) In the numerical simulation, the FEM model used by the ABAQUS/Explicit software adopted the Kim-Tuan equation; the Hill 1948 yield function offered good results of fracture prediction in the mean of fracture depth and fracture position.

Acknowledgments

This research was supported by Basic Science Research Program through the National Research Foundation of Korea (NRF) funded by the Ministry of Education (2017R1A6 A3A11030503). In addition, this work was partly supported by the Korea Institute of Energy Technology Evaluation and Planning (KETEP) and the Ministry of Trade, Industry & Energy (MOTIE) of the republic of Korea (grant No. 20155000000100).

References

[1] H. Iseki, K. Kato and S. Sakamoto, Flexible and incremental sheet metal bulging using a path-controlled spherical roller, *Transactions of the Japan Society of Mechanical Engineers Series C*, 504 (58) (1992) 3147-3155.

[2] M. Ham and J. Jeswiet, Single point incremental forming and forming criteria for AA3003, *CIRP Annals - Manufacturing Technology,* 55 (1) (2006) 241-244.

[3] A. Bhattacharya, K. Maneesh, N. Venkata and J. Cao, Formability and surface finish studies in single point incremental forming, *Journal of Manufacturing Science and Engineering,* 133 (6) (2011).

[4] T. Obikawa, T. Hakutani, T. Sekine, S. Numajiri, T. Matsumura and M. Yoshino, Single-point incremental microforming of thin shell products utilizing high formability, *Journal of Advanced Mechanical Design, Systems, and Manufacturing*, 6 (4) (2010) 1145-1156.

[5] J. Cao and R. Malhotra, System and method for accumulative double sided incremental forming, *US Patent*, 9168580B2 (2015).

[6] T. H. D. Nguyen, H. S. Oh, S. T. Hong, H. N. Han and J. Cao, A review of electrically-assisted manufacturing, *International Journal of Precision Engineering and Manufacturing-Green Technology*, 2 (4) (2015) 365-376.

[7] M. Durante, A. Formisano, A. Langella and M. C. Minutolo, The influence of tool rotation on an incremental forming process, *Journal of Materials Processing Technology,* 209 (9) (2009) 4621-4626.

[8] J. Wang, L. H. Li and H. S. Jiang, Effects of forming parameters on temperature in frictional stir incremental sheet forming, *Journal of Mechanical Science and Technology,* 30 (5) (2016) 2163-2169.

[9] M. S. Mohamed, A. D. Foster, J. G. Lin, D. S. Balint and T. A. Dean, Investigation of deformation and failure features in hot stamping of AA6082: Experimentation and modelling, *International Journal of Machine Tools and Manufacture*, 53 (1) (2012) 27-38.

[10] H. Wang, Y. B. Luo, P. Friedman, M. H. Chen and L. Gao, Warm forming behavior of high strength aluminum alloy AA7075, *Transactions of Nonferrous Metals Society of China*, 22 (1) (2012) 1-7.

[11] W. C. Xiao, B. Y. Wang, Y. Kang, W. P. Ma and X. F. Tang, Deep drawing of aluminum alloy 7075 using hot stamping, *Rare Metals*, 36 (6) (2017) 485-493.

[12] Q. T. Pham, B. H. Lee, K. C. Park and Y. S. Kim, Influence of the post-necking prediction of hardening law on the theoretical forming limit curve of aluminium sheets, *International Journal of Mechanical Science,* 140 (2018) 521-536.

[13] J. Jeswiet, F. Micari, G. Hirt, A. Bramley, J. Duflou and J. Allwood, Asymmetric single point incremental forming of sheet metal, *CIRP Annals - Manufacturing Technology*, 54 (2) (2005) 88-114.

[14] D. Young and J. Jeswiet, Forming limit diagrams for single point incremental forming of aluminum sheet, *Proc. of the Institution of Mechanical Engineers Part B: Journal of Engineering Manufacture*, 4 (219) (2005) 359-364.

[15] M. Durante, A. Formisano and A. Langella, Observations on the influence of tool-sheet contact conditions on an incremental forming process, *Journal of Materials Engineering and Performance*, 20 (6) (2011) 941-946.

[16] G. Hussain, N. Hayat and L. Gao, Pyramid as test geometry to evaluate formability in incremental forming: Recent results, *Journal of Mechanical Science and Technology,* 26 (8) (2012) 2337-2345.

[17] M. B. Silva, K. Isik, A. E. Tekkaya and P. A. F. Martins, Fracture loci in sheet metal forming: a review, *Acta Metallurgica Sinica,* 28 (12) (2015) 1415-1425.

[18] V. C. Do, Q. T. Pham and Y. S. Kim, Identification of forming limit curve at fracture in incremental sheet forming, *International Journal of Advanced Manufacturing Technology*, 92 (9-12) (2017) 4445-4455.

Xiao Xiao is a Ph.D. student at Kyungpook National University, Republic of Korea. He received his Master degree at Kyungpook National University, Korea in 2017. His research interests are plasticity, sheet metal forming and FEM.

Young-Suk Kim received his M.S. degrees from the Department of Mechanical Engineering at Seoul National University in 1981. He obtained his Ph.D. degree from the Department of Mechanical Engineering at Kobe University in 1986. He is currently a Professor in the Department of Mechanical Engineering at Kyungpook National University. His research interests are production engineering, plasticity, nano / micromechanics, FEM and biomechanics.